RSC Advances

ROYAL SOCIETY OF CHEMISTRY

www.rsc.org/advances

Synthesis and optical properties of the composite films from P3HT and sandwich-like Ag-C-Ag nanoparticles

Lingpeng Yan,[ab] Yamin Hao,[ab] Xiaoting Feng, [ab] Yongzhen Yang,*[ab] Xuguang Liu *[abc] Yongkang Chen [ad] and Bingshe Xu [ab]

[a] Key Laboratory of Interface Science and Engineering in Advanced Materials, Ministry of Education, Taiyuan University of Technology, Taiyuan 030024, China

[b] Research Center of Advanced Materials Science and Technology, Taiyuan University of Technology, Taiyuan 030024, China

[c] College of Chemistry and Chemical Engineering, Taiyuan University of Technology, Taiyuan 030024, China

[d] University of Hertfordshire, School of Engineering and Technology, Hatfield, Herts. AL10 9AB, UK

Abstract

Sandwich-like Ag-C-Ag nanoparticles (Ag-C-Ag NPs) were mildly synthesized under hydrothermal conditions in one step method. With this approach, Ag was not only encapsulated in the centre of an individual carbon nanosphere and was also uniformly dispersed within the carbon matrix up to the sphere's shell. Then, poly(3-hexylthiophene): Ag-C-Ag NPs (P3HT:Ag-C-Ag NPs) composite films were prepared by a spin coating method with a mixture chlorobenzene solution of Ag-C-Ag NPs and P3HT. Both morphology and microstructure of Ag-C-Ag NPs were investigated by field emission scanning electron microscopy and high resolution transmission electron microscopy. The possible formation mechanism was proposed. The results have indicated that the Ag-C-Ag NPs present many functional groups and their energy level matches with that of P3HT. It has been observed that an introduction of Ag-C-Ag NPs to P3HT can induce broad and high absorbing spectra as well as a great photoluminescence quenching of P3HT. It is evident that sandwich-like Ag-C-Ag NPs have a great potential to be a new acceptor material in photovoltaic devices.

Keywords: Sandwich-like Ag-C-Ag nanoparticles; Fabrication; Composite film; Optical performance

1. Introduction

Hybird nanoparticles or sub-microparticles represent a new kind of structure, the structure has attracted much attention in recent years. The hybrid structure possesses improved physical and chemical properties over its single-component counterparts [1-8], such as remarkably enhanced photoluminescence efficiency and prominent catalytic property in specific reactions, which may widen its potential applications in electronics, magnetism, optics, and catalysis.

Metal materials have also been reported to increase light absorption in active layers of solar cells (SCs) with their plasma effects [9-11]. At the nano-scale, metallic nanoparticles can be penetrated by electromagnetic waves, which induce a separation of charges and consequently a coherent oscillation (surface plasmon). Surface plasmons are essentially light waves that are trapped on the surfaces because of their interaction with the free electrons of the metal [12]. The primary consequences of excitation due to localized surface plasmon resonance are selective photo absorption, scattering, and local electromagnetic field enhancement [13]. Silver (Ag) exhibits highest electrical and thermal conductivities among all types of metal and has a good property of oxidation resistance. Its optical trapping potential is also most effective owing to its high scattering efficiency in a visible range [14]. However, silver nanoparticles are prone to coalesce as a result of van der waals forces and high surface energy unless they are protected [2]. Carbon nanospheres have been proposed to provide a role in protection.[15] As a part of the carbon family, carbon nanospheres, which have stable chemical, thermal properties and low preparation cost, are promising to be used as a metal support.

Sun and Li [16] got Ag/C core/shell spheres using water as environmentally benign solvent. Carbon nanospheres loading silver nanoparticles were also obtained by two-step methods [17, 18]. Though Wang et al [17] investigated a new synthesis route of Ag/C core/shell nanospheres with many small Ag particles on the surface of a shell structure, the synthesis steps were complex and not so eco-friendly.

In this study, sandwich-like Ag-C-Ag nanoparticles (Ag-C-Ag NPs), with Ag encapsulated in the middle of a carbon nanosphere, distributed in the carbon shell and loaded on the surface of the carbon sphere, were synthesized in one step under typical hydrothermal conditions. Their application as an acceptor for polymer solar cells with P3HT as the donor becomes attractive in this study. This composite structure is

expected to yield an enhanced and broader absorption range of the solar spectrum that could induce a remarkable increase in charge generation. Ultraviolet-visible (UV-vis) and photoluminescence (PL) spectroscopies were used to confirm the optical behaviour.

2. Experimental

2.1 Preparation of sandwich-like Ag-C-Ag NPs

In a typical preparation, 30 ml of 0.4 M aqueous glucose solution was added to a 50 ml Teflon liner, then 2 ml of 0.03 M $AgNO_3$ aqueous solution was added dropwise under vigorous stirring. Having been ultrasonicated for 20 minutes, the mixture of solution was placed in an autoclave. The autoclave was heated to a certain temperature (180, 190 and 200℃), kept at this selected temperature for 4 hours and then cooled to room temperature. The resulting salmon precipitate was collected through centrifugation and washed with distilled water and absolute alcohol for several times. The product was redispersed in absolute ethanol and subsequently dried at 50℃ for 24 hours in an oven.

2.2 Fabrication of P3HT:Ag-C-Ag NPs composite films

Regioregular P3HT was provided commercially by Luoyang Microlight Material Technology Co., Ltd and used without further purification. 10 mg of P3HT were diluted in 1 ml of chlorobenzene, then 0, 2.5, 5 and 10 mg of Ag-C-Ag NPs were added in the above solutions separately. P3HT and Ag-C-Ag NPs in the mass ratio of 1:0, 4:1, 2:1, 1:1 were mixed in solution sates. Then the mixture solutions were magnetically stirred for 12 hours.

Glass substrates were precleaned repeatedly in an ultrasonic bath and sequentially cleaned by detergent, deionized water, ethanol and acetone respectively. The P3HT:Ag-C-Ag NPs solution was spin-coated onto the cleaned glass substrate at a spin rate of 1000 rpm for 1 minute and dried under the room temperature.

2.3 Materials characterization

The morphologies of the samples were characterized by a JSM-6700F field

emission scanning electron microscopy (FESEM) at 10 kV, whose specification includes an acceleration voltage range of 0.5~30 kV and a beam intensity range of 10^{-13}~2×10^{-9} A. The samples were coated with gold (Au) in an evaporator to avoid charging during electron irradiation. The structures of the products were observed with a JEM-2010 high resolution transmission electron microscopy (HRTEM), a Tenror 27 Fourier transformation infrared spectrometer (FTIR) and a D8 Advance x-ray diffractometer (XRD). The thermal stability of the samples was characterized by thermogravimetry (Netzsch TG 209F3) operating in air atmosphere from 100℃ to 900℃ at a heating rate of 10℃/min. To obtain the electronic structure of the Ag-C-Ag NPs, a cyclic voltammetry (CV) analysis was conducted with a CS350 electrochemical workstation using a Pt disk, Pt wire and calomel electrode as working electrode, counter electrode and reference electrode, respectively, and using tetrabutylammonium perchlorate (TBAP, 0.1 M) dimethyl formamide as supporting electrolyte. The U-3900 ultraviolet-visible spectrophotometer (UV-Vis) and Fluoromax-4 photoluminescence spectrometer (PL) were employed to characterize the optical property of the composite.

3. Results and discussion

3.1 Characterization of sandwich-like Ag-C-Ag NPs

The Ag-C-Ag NPs were prepared by hydrothermal method at different temperatures, as shown in Fig. 1. It can be seen from TEM images of samples that the as-synthesized products have different morphologies and structures. The carbon nanospheres were severely agglomerated and contained barely any Ag nanoparticles as shown in Fig. 1(a). This suggests that Ag^+ did not participate in a chemical reaction at low temperature of 180℃. As shown in Fig. 1(b), when the temperature was 190℃, the typical sandwich-like Ag-C-Ag NPs were formed and the Ag nanoparticles were encapsulated in the middle of carbon spheres, distributed in the carbon shell and loaded on the surfaces of the carbon spheres. This illustrates that Ag^+ was gradually reduced into Ag nanoparticles at the temperature of 190℃, and the Ag nanoparticles were also spread within the carbon nanospheres besides Ag nanoparticles encapsulated in carbon spheres. However, Ag^+ was reduced fast at the temperature of 200℃, and Ag nanoparticles were only encapsulated in carbon spheres, as shown in

Fig. 1(c). In general, the optimum temperature of obtaining Ag-C-Ag NPs is 190℃.

Fig. 2(a) gives a typical FESEM image of Ag-C-Ag NPs, which exhibits regular spherical shapes with diameters in a range from 300 to 520 nm. Energy Dispersive Spectroscopy (EDS) indicates that the sandwich-like structure consists of C, O and Ag, as shown in the top right corner of Fig. 2(a). To further investigate the detailed structure of the products, TEM analyses were conducted. Firstly, it can be distinctly seen from Fig. 2(b) that Ag particles (arrow A) are encapsulated in the carbon shell, and the diameter of core and the thickness of the shell are about 80 and 200 nm, respectively. Secondly, Fig. 2(b) also shows that the Ag nanoparticles (about 20 nm in size) dispersed in the carbonaceous matrix can be divided into two parts with different distributions. The first part is on the surface of the carbon shell with the crystal spacing of 0.23 nm corresponding to Ag (111), as marked by square in Fig. 2(b) and showed in an inset at the bottom left corner of Fig. 2(c). As shown in an inset at the top left corner of Fig. 2(c), the electron diffraction pattern indicates the single-crystalline nature of the Ag nanoparticles. It can also be observed that a thin layer of carbon (less than 2 nm) surrounds the Ag nanocrystals. The second part is dispersed inside the carbon matrix (arrow B in Fig. 2(b)). Thirdly, a small amount of hollow spheres without an Ag nanoparticle core or with a split Ag nanoparticle core was found, as marked with the circles in Figs. 2(b) and (d). More importantly, compared with the carbon spheres with a full Ag nanoparticle core, these hollow spheres without an Ag nanoparticle core or with a split Ag nanoparticle core have more Ag nanoparticles dispersed in the carbon matrix.

Fig. 3 presents the XRD profiles of Ag-C-Ag NPs. It can be seen that there is a broad peak in the range of 15 to 30°, which is attributed to (002) reflection of a carbon layer in Ag-C-Ag NPs, indicating the existence of amorphous carbon. It is found that strong diffraction peaks assigned to Ag nanocrystals at 8.15°, 44.30°, 64.45° and 77.30° are associated with the (111), (200) (220) and (311) reflections of Ag nanocrystals, respectively, illustrating that the Ag nanocrystals are stacked in what is known as a face-centred aubic structure. Otherwise, the strongest diffraction peak of Ag nanocrystals is the (111) reflection, indicating that the preferable growth face of Ag nanocrystals is in (111).

In order to determine the ratio of Ag nanocrystals in Ag-C-Ag NPs and thermal stability of Ag-C-Ag NPs, a TG test in air was carried out. As can be seen in Fig. 4,

Ag-C-Ag NPs exhibit only 5.50% of weight loss when the temperature rose up to 275℃. When the temperature exceed 285□, the Ag-C-Ag NPs begun to lose weight fast and reached a steady status above 380℃. During the period of the fast weight loss, carbon plies were oxidized to carbon dioxide, and eventually, the oxidization and deoxidization of Ag nanocrystals was in equilibrium. The final product is Ag nanocrystals at last because Ag_2O is unstable at high temperatures. Thus the ratio of Ag nanocrystals in Ag-C-Ag NPs is about 5.30%.

FTIR measurements were carried out to investigate the functional groups of products after a hydrothermal treatment. As shown in Fig. 5, the bands at 1701 and 1625 cm^{-1} were attributed to C=O and C=C vibrations, respectively, indicating the aromatization of glucose during the hydrothermal treatment. It can be seen that the as-synthesized Ag-C-Ag NPs had a strong band of –OH (O–H stretching vibrations) at 3429 cm^{-1}, along with the weak peaks of C-OH at 1385 and 1302 cm^{-1}, which means that as-synthesized Ag-C-Ag NPs are rich in hydroxyl. The presence of a functional group makes Ag-C-Ag NPs disperse better in aqueous medium and common organic solvents, which can greatly widen the range of their applications.

3.2 Formation mechanism of sandwich-like Ag-C-Ag NPs

A possible formation mechanism is schematically illustrated in Fig. 6. There are four stages. Initially, Ag^+ did not react with glucose under the ambient condition. However, as the solution was sealed in autoclaves and heated to 190-200℃, Ag^+ was reduced by glucose under hydrothermal conditions. At the beginning stage as shown in Fig. 6(a), most of the silver ions in the solution was deoxidized by glucose and Ag nanoparticles were nucleated[7, 16]. In the following stage shown in Fig. 6(b), carbon shells were formed by in-suit deposition of carbonaceous products around the surface of an Ag core with Ag nanoparticles catalysing the carbonization of glucose[7, 19]. In the third stage shown in Fig. 6(c), as reaction proceeded, the unreacted Ag^+ in the reaction system was gradually reduced into Ag nanoparticles. The Ag nanoparticles were evenly dispersed in the solution system with reactive surfaces, which catalyzed the following carbonization of glucose and led to gradual embedding in the carbon matrix of the Ag nanoparticles along with the carbonization of glucose, as indicated by the TEM images of Ag-C-Ag NPs marked with arrow B in Fig. 2(b). In the final stage

shown in Fig. 6(d), Ag nanoparticles loaded on the surface of a carbon shell (as marked with square in Fig. 2(b) were obtained by the subsequent reduction of redundant Ag^+.

Based upon an analysis of Zeta potential on the products, the surfaces of the Ag-C-Ag NPs have been negatively charged in water (pH=7, ξ= -25 eV). This negative charge was originated from the ionization of the –COOH and –OH on the surface of Ag-C-Ag NPs[20]. A small amount of hollow or split nanoparticles, as marked by the circles in Figs. 2(b) and 2(d), may be induced by the electrostatic suction between a Ag core with positive electricity and a carbon matrix[19]. Under the action of electrostatic attraction, Ag nanoparticles were diffused from the core into the carbonaceous matrix, resulting in the spliting of the Ag core and the presence of trace amounts of hollow or split Ag nanoparticles, as shown in Figs. 6(e)-6(f). Thus, it can be reasonably suggested that some of Ag nanoparticles dispersed in the carbon matrix and on the surface of carbon shell were originated from the outward diffusion of Ag nanoparticles under electrostatic forces. This is also verified by the fact that carbon spheres with a hollow or split Ag nanoparticle core have more Ag nanoparticles dispersed in the carbon matrix than the carbon spheres with full Ag cores, as shown in the circles of Fig. 2(b) and Fig. 2(d). Therefore, it is suggested that the formation of Ag nanoparticles dispersed in the carbon matrix and on the surface of carbon shell may include two reasons: a reduction of Ag^+ and outward diffusion of the Ag nanoparticles under electrostatic forces.

3.3 Feasibility analysis of a potential application

To explore a potential application of the Ag-C-Ag NPs and Ag nanoparticles encapsulated in carbon spheres (Ag@C NPs) in photovoltaic cells, a CV test of Ag-C-Ag NPs and Ag@C NPs was carried out for determination of their band gap energies. As shown in Fig. 7, both HOMO and LUMO energy levels were estimated from their onset oxidation potential and reduction potential according to Equations (1) and (2) [21] as follows:

$$\text{HOMO} = -(E_0^{ox} + 4.74)\ (\text{eV}), \quad (1)$$

$$\text{LUMO} = -(E_0^{red} + 4.74)\ (\text{eV}), \quad (2)$$

where E_0^{ox} and E_0^{red} are the onset oxidation potential and onset reduction potential, respectively.

It can be seen in Fig. **7** that E_0^{ox} and E_0^{red} of Ag@C NPs are 0.95 V and -0.06 V, respectively. Therefore, the calculated HOMO and LUMO energy levels are -5.69 and -4.68 eV, respectively. Eg, the difference between HOMO and LUMO energy levels, is calculated to be 1.01 eV. Similarly, the HOMO level, LUMO level and Eg of Ag-C-Ag NPs are calculated as -5.55, -4.40 and 1.15 eV. Free holes and electrons cannot be created directly in composite films when light is absorbed because excitons have a large binding energy of 0.3 eV [22], so the energy gaps of electron donors and electron acceptors ΔE_1 and ΔE_3 should be greater than 0.3 eV, where $\Delta E_1=D_{LUMO}-A_{LUMO}$, $\Delta E_3=D_{HOMO}-A_{HOMO}$, D refers to electron donors and A refers to electron acceptors. It has been reported that the HOMO and LUMO of P3HT are -5.0 and -3.0 eV [19], respectively. As a result, ΔE_1 and ΔE_3 of the active layer based on electron-donating P3HT and electron-accepting Ag@C NPs are 0.69 and 1.68 eV, respectively, and those of the active layer based on electron-donating P3HT and electron-accepting Ag-C-Ag NPs are 0.55 and 1.40 eV, respectively. Both are greater than the exciton binding energy. Therefore, it is suggested that Ag@C NPs and Ag-C-Ag NPs could be suitable to be used as the acceptor materials of polymer solar cells. For donor–acceptor bulk heterojunction solar cells, the V_{oc} value is mainly determined by the difference between the acceptor's LUMO level and the donor's HOMO level [23], which can be expressed as follows:

$$V_{oc}=e^{-1}\times(\,|\,HOMO^{donor}\,|-|\,LUMO^{acceptor}\,|\,-0.3\ eV\,) \qquad (3)$$

In the active layers, the HOMO level for P3HT is -5.0 eV, the LUMO levels of Ag@C NPs and Ag-C-Ag NPs are -4.68 and -4.40 eV, respectively. Thus the V_{oc} values of P3HT: Ag@C and P3HT: Ag-C-Ag NPs are determined to be 0.32 and 0.60 V, according to Equation (3). It can be suggested from the V_{oc} values of P3HT: Ag@C and P3HT: Ag-C-Ag NPs that Ag-C-Ag NPs are more suitable for active materials of photovoltaic cells.

3.4 Optical properties of P3HT: Ag-C-Ag NPs composite films

To further investigate a possible application of Ag-C-Ag NPs in an active layer, the P3HT:Ag-C-Ag NPs mixture solutions were spin-coated on quartz and

characterized by UV-Vis and PL. The PL spectra of pure P3HT, Ag-C-Ag NPs and composite films with different mass ratios were studied, with emphasis on quenching phenomena in order to compare their efficiencies of a photo-induced charge transfer. The PL spectra were obtained at an excitation wavelength of 420 nm in the range from 500 to 820 nm. It is evident from Fig. 8 that when Ag-C-Ag NPs were introduced into the P3HT, the PL intensity of the composite films was significantly quenched. The quenching suggests a photo-induced charge transfer in the composite films [24]. This implies that electrons and holes are separated effectively and transferred in their interpenetrating phase. The quenching phenomena are more obvious when the mixing ratios are 2:1 and 1:1. Fig. 8 also shows a few minor peaks which indicate that some of the excited electrons of P3HT were radiatively decayed without a completion of a charge transfer to the acceptor [25]. The outcome from the PL quenching test suggests that the Ag-C-Ag NPs may accept electrons efficiently from the P3HT donor polymer.

Fig. 9 shows the morphology of a typical P3HT:Ag-C-Ag NPs (2:1; w/w) composite film. As can be seen from the TEM image of the composite film, the sandwich-like Ag-C-Ag NPs can also been observed clearly, as consistent with the TEM image of Ag-C-Ag NPs, and they have a good dispersion in P3HT, attributed to good solubility of Ag-C-Ag NPs in chlorobenzene. This good dispersion contributes to the formation of an interpenetrating network structure in the composite film, which is conducive to the efficient transfer of photo-induced charge in the composite film. This result is in a good agreement with the PL characterization results shown in Fig. 8.

To investigate the optical properties of P3HT:Ag-C-Ag NPs composite films, the UV-Vis absorption spectra of P3HT:Ag-C-Ag NPs (2:1; w/w) were investigated. Besides, Ag-C-Ag NPs prepared at 180℃ (Ag-C-Ag NPs-180) were used for a comparison, which contain barely any Ag nanoparticles. Fig. 10 shows the UV-Vis absorption spectra of P3HT, P3HT:Ag-C-Ag NPs (2:1; w/w), P3HT:Ag-C-Ag NPs-180 (2:1; w/w) and the difference spectra between the composite films and P3HT in the solid state. In the spectrum of pure P3HT, the highest energy peak exists at 526 nm. Two shoulders can also be found at 553 and 599 nm, which represent vibrational excitations of crystalline P3HT. After pure P3HT is blended with the P3HT:Ag-C-Ag NPs-180, the absorbance of the composite film in the region of 400-700 nm is weakly

increased, because the Ag-C-Ag NPs-180 have weak absorption. However, after introduction of Ag-C-Ag NPs, the absorption of P3HT:Ag-C-Ag NPs composite films show an obvious enhancement in the range of 300-650 nm, which is likely attributed to the plasma resonances of Ag-C-Ag NPs. In addition, by comparing the difference spectra of P3HT with P3HT:Ag-C-Ag NPs and P3HT:Ag-C-Ag NPs-180, the stronger absorption of P3HT:Ag-C-Ag NPs can also be revealed.

To study the plasmon resonance of Ag-C-Ag NPs, the UV-Vis absorption spectra of Ag-C-Ag NPs (5 mg/mL, 1000 rpm) and Ag-C-Ag NPs-180 (5 mg/mL, 1000 rpm) in solid state were characterized, as shown in Fig. 11. In comparison with Ag-C-Ag NPs-180, the Ag-C-Ag NPs show much more intensive light absorption bands in the ranges of 300-650 nm, which is consistent with the difference spectra of P3HT:Ag-C-Ag NPs and P3HT, suggesting the existence of plasmon in P3HT:Ag-C-Ag NPs film. Silver nanoparticles can absorb visible light intensely because of the surface plasmon resonance effect[26], so the Ag-C-Ag NPs show more intensive light absorption than Ag-C-Ag NPs-180. The spectral enhancement is likely due to two major factors. The first could be a local enhancement of the electromagnetic field on an account of localized surface plasmon resonances [27, 28]. The other could be the plasmon resonance scattering which becomes dominant when a larger Ag core is used. It appears that the scattering lengthens the optical path several times in the active layer, thereby enhancing the degree of light absorption [29].

4. Conclusions

Synthesis and optical properties of the composite films from P3HT and sandwich-like Ag-C-Ag nanoparticles have been investigated. Based on the above results and discussion, the following conclusions can be drawn:

i) Sandwich-like Ag-C-Ag NPs were hydrothermally synthesized with one step method and the possible formation mechanism of Ag-C-Ag NPs was proposed. With this method, Ag was not only encapsulated in the centre of a carbon nanosphere and also uniformly dispersed within the carbon matrix and on the carbon nanosphere's shell.

ii) The ratio of Ag nanocrystals in Ag-C-Ag NPs is about 5.30% and the Ag-C-Ag NPs present many functional groups. These groups facilitate them further functionalization and various applications.

iii) With a matched energy level, the Ag-C-Ag NPs and P3HT composite films possess apparent quenching phenomena indicating an efficiently photoinduced charge transfer in the composite films, and enhanced absorption in the optical range, which is due to the plasmon resonances of Ag nanoparticles in Ag-C-Ag NPs. Therefore, sandwich-like Ag-C-Ag NPs have a great potential to be a new highly efficient acceptor material for an application in polymer solar cells.

Author information

Corresponding Author

*E-mail: Yongzhen Yang: yyztyut@126.com;

Xuguang Liu: liuxuguang@tyut.edu.cn

Notes

The authors declare no competing financial interest.

Acknowledgments

The authors would like to thank Suzhou Institute of Nano-Tech and Nano-Bionics, Chinese Academy of Sciences for high resolution transmission electron microscopy test. The authors acknowledge financial support from National Natural Science Foundation of China (21176169), Shanxi Provincial Key Innovative Research Team in Science and Technology (2012041011), International Science & Technology Cooperation Program of China (2012DFR50460), Research Project Supported by Shanxi Scholarship Council of China (2012-038), Post-graduate Innovation Program of Shanxi Province (20143010), Post-graduate Innovation Foundation of Taiyuan University of Technology (S2014103) and Open Foundation project of Key Laboratory of Interface Science and Engineering in Advanced Materials (Taiyuan University of Technology) (KLISEAM201502).

References and Notes

1. J. Cheng, Y. Wang, C. Teng, Y. Shang, L. Ren and B. Jiang, *Chem. Eng. J.*, 2014, 242, 285-293.
2. J. Lee, K. Han and D.J. Jang, *Applied Catalysis A: General*, 2014, 469, 380-386.
3. V. K. Gupta, M. L. Yola, T. Eren, F. Kartal, M. O. Çağlayan and N. Atar, *J. Mol. Liq.*, 2014, 190, 133-138.
4. M. K. Joshi, H. R. Pant, H. J. Kim, J. H. Kim and C. S. Kim, *Colloids and Surfaces A: Physicochemical and Engineering Aspects*, 2014, 446, 102-108.
5. S. Yang, C. Nie, H. Liu and H. Liu, *Mater. Lett.*, 2013, 100, 296-298.

6. S. Mao, W. Li, Y. Long, Y. Tu and A. Deng, *Anal. Chim. Acta*, 2012, 738, 35-40.
7. S. Y. Wu, Y. S. Ding, X. M. Zhang, H. O. Tang, L. Chen and B. X. Li, *J. Solid State Chem.*, 2008, 181, 2171-2177.
8. Y. D. Han, J. W. Lee, D. H. Park, S. H. Yang, B. K. Kim, J. Kim and J. Joo, *Synth. Met.*, 2011, 161, 2103-2106.
9. L. Chen, S. Zhang, L. Chang, L. Zeng, X. Yu, J. Zhao, S. Zhao and C. Xu, *Electrochim. Acta*, 2013, 93, 293-300.
10. V. E. Ferry, J. N. Munday and H. A. Atwater, *Adv. Mater.*, 2010, 22, 4794-4808.
11. H. A. Atwater and A. Polman, *Nature Materials*, 2010, 9, 205-213.
12. W. L. Barnes, A. Dereux and T. W. Ebbesen, *Nature*, 2003, 424, 824-830.
13. T. R. Jensen, M. D. Malinsky, C. L. Haynes and R. P. Van Duyne, *The Journal of Physical Chemistry B*, 2000, 104, 10549-10556.
14. X. Li, W. C. H. Choy, H. Lu, W. E. Sha and A. H. P. Ho, *Adv. Funct. Mater.*, 2013, 23, 2728-2735.
15. J. Cui, C. Hu, Y. Yang, Y. Wu, L. Yang, Y. Wang, Y. Liu and Z. Jiang, *J. Mater. Chem.*, 2012, 22, 8121-8126.
16. X. Sun and Y. Li, *Angew. Chem. Int. Ed.*, 2004, 43, 597-601.
17. H. Wang, Q. Jin, L. Yang and Y. Liu, *J. Nanopart. Res.*, 2013, 15, 1-9.
18. Y. Zhao, Z.Q. Wang, X. Zhao, W. Li and S.X. Liu, *Appl. Surf. Sci.*, 2013, 266, 67-72.
19. C. Li, Y. Zhu, X. Zhang, X. Yang and C. Li, *RSC Advances*, 2012, 2, 1765-1768.
20. B. Zhang, C. Y. Liu and Y. Liu, *Eur. J. Inorg. Chem.*, 2010, 2010, 4411-4414.
21. Y. Li, L. Yan, Y. Yang, X. Liu and B. Xu, *J. Mater. Res.*, 2014, 29, 492-500.
22. J. Subbiah, C. M. Amb, I. Irfan, Y. Gao, J. R. Reynolds and F. So, *ACS applied materials & interfaces*, 2012, 4, 866-870.
23. Y. Li, Y. Hu, Y. Zhao, G. Shi, L. Deng, Y. Hou and L. Qu, *Adv. Mater.*, 2011, 23, 776-780.
24. S. M. Abdullah, Z. Ahmad, F. Aziz and K. Sulaiman, *Org. Electron.*, 2012, 13, 2532-2537.
25. H. U. Kim, D. Mi, J. H. Kim, J. B. Park, S. C. Yoon, U. C. Yoon and D. H. Hwang, *Sol. Energy Mater. Sol. Cells*, 2012, 105, 6-14.
26. S. Sun, W. Wang, L. Zhang, M. Shang and L. Wang, *Catal. Commun.*, 2009, 11, 290-293.
27. I. Ding, J. Zhu, W. Cai, S. J. Moon, N. Cai, P. Wang, S. M. Zakeeruddin, M. Grätzel, M. L. Brongersma and Y. Cui, *Advanced Energy Materials*, 2011, 1, 52-57.
28. S. Pillai and M. Green, *Sol. Energy Mater. Sol. Cells*, 2010, 94, 1481-1486.
29. J. L. Wu, F. C. Chen, Y.S. Hsiao, F. C. Chien, P. Chen, C. H. Kuo, M. H. Huang and C. S. Hsu, *Acs Nano*, 2011, 5, 959-967.

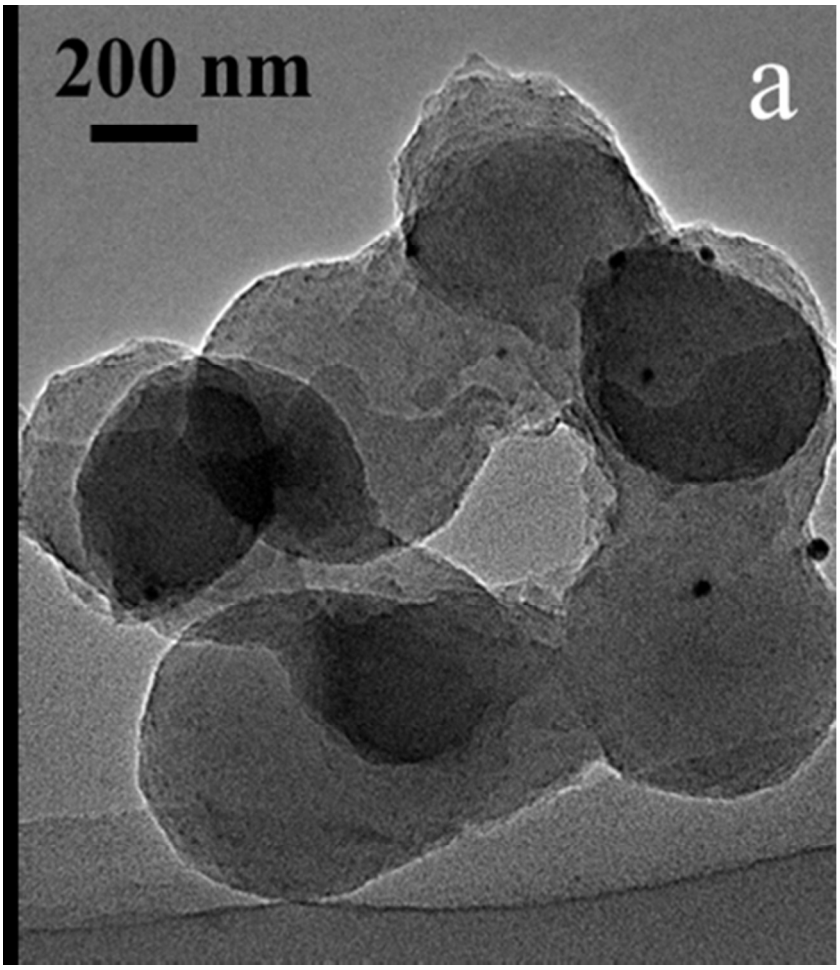

Fig. 1(a) TEM images of Ag-C-Ag NPs prepared at 180℃
70x81mm (150 x 150 DPI)

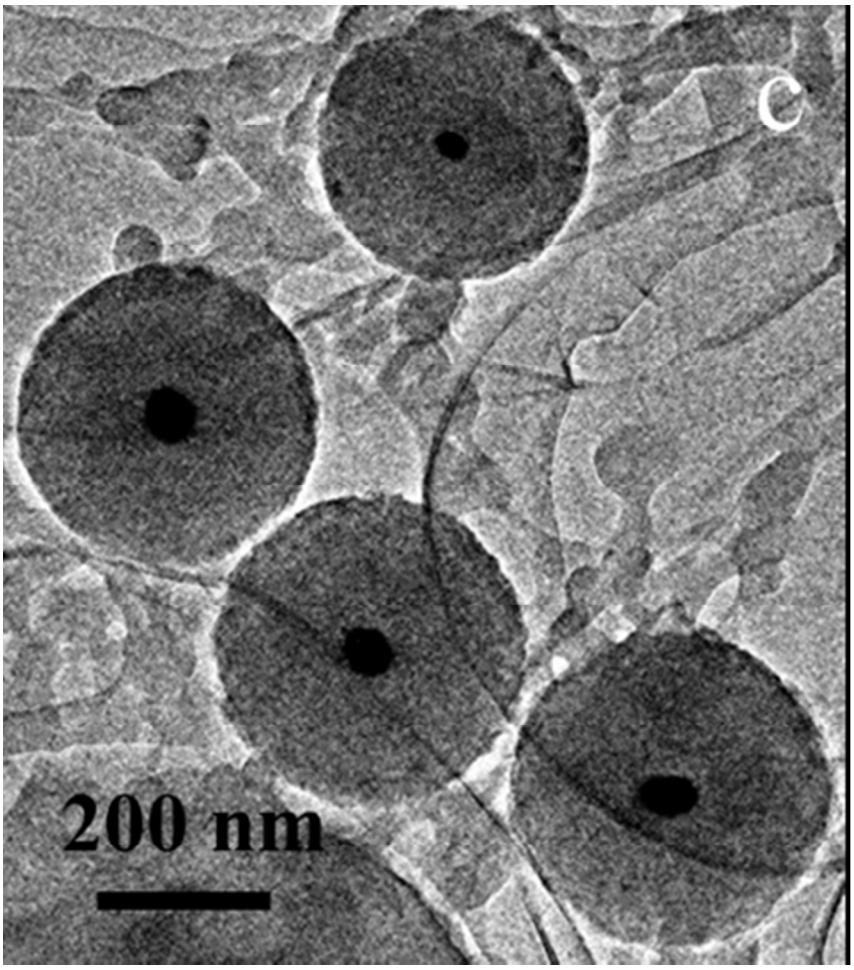

Fig. 1(c) TEM images of Ag-C-Ag NPs prepared at 200℃
71x81mm (150 x 150 DPI)

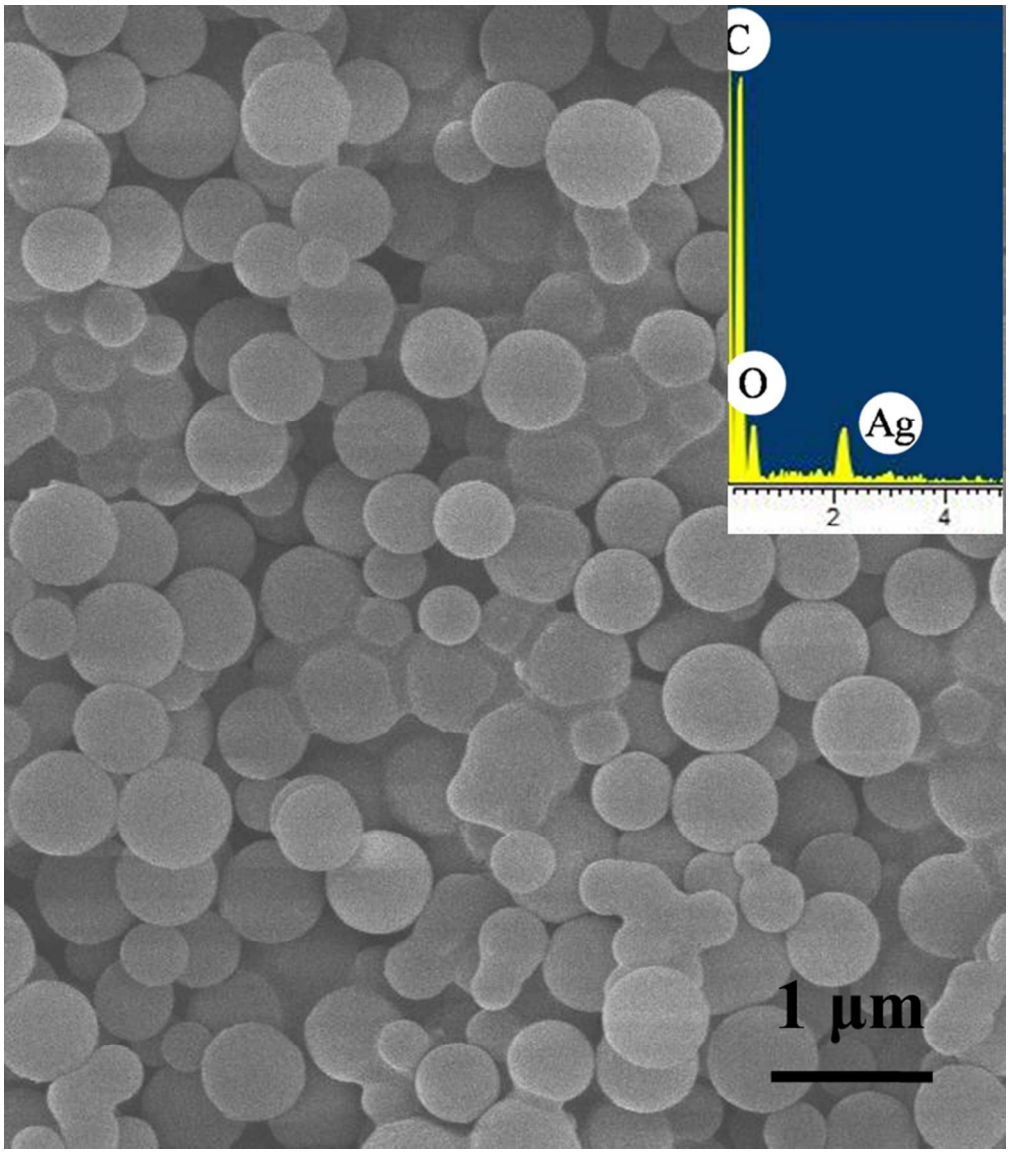

Fig. 2 (a) FESEM image of Ag-C-Ag NPs (Inset is EDS spectrum)
140x160mm (150 x 150 DPI)

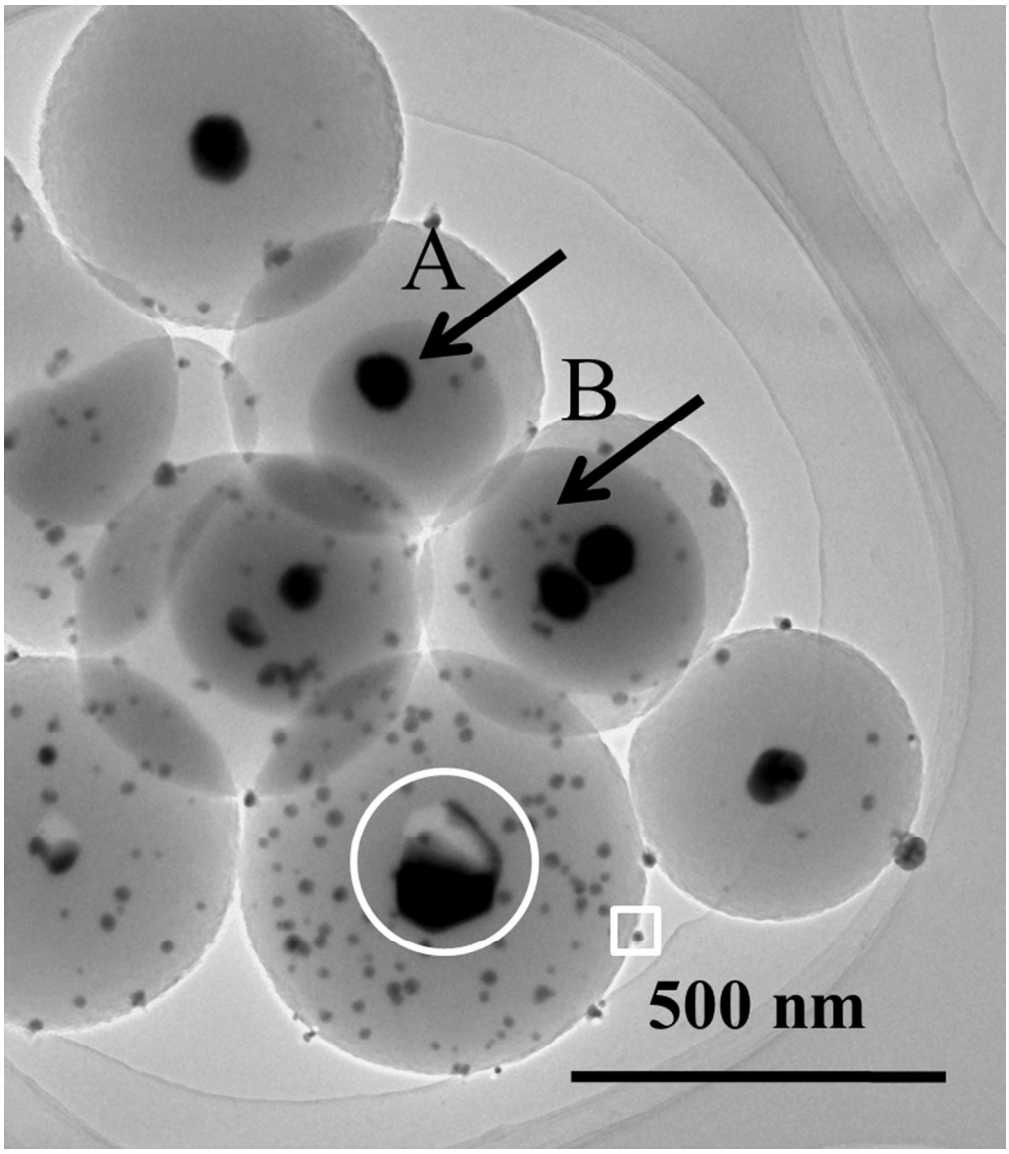

Fig. 2 (b) TEM images of the products: carbon-encapsulated Ag nanoparticles as indicted by the arrow A, dispersed Ag nanoparticles as indicated by the arrow B, split Ag nanoparticles as indicated by the circle, 140x160mm (150 x 150 DPI)

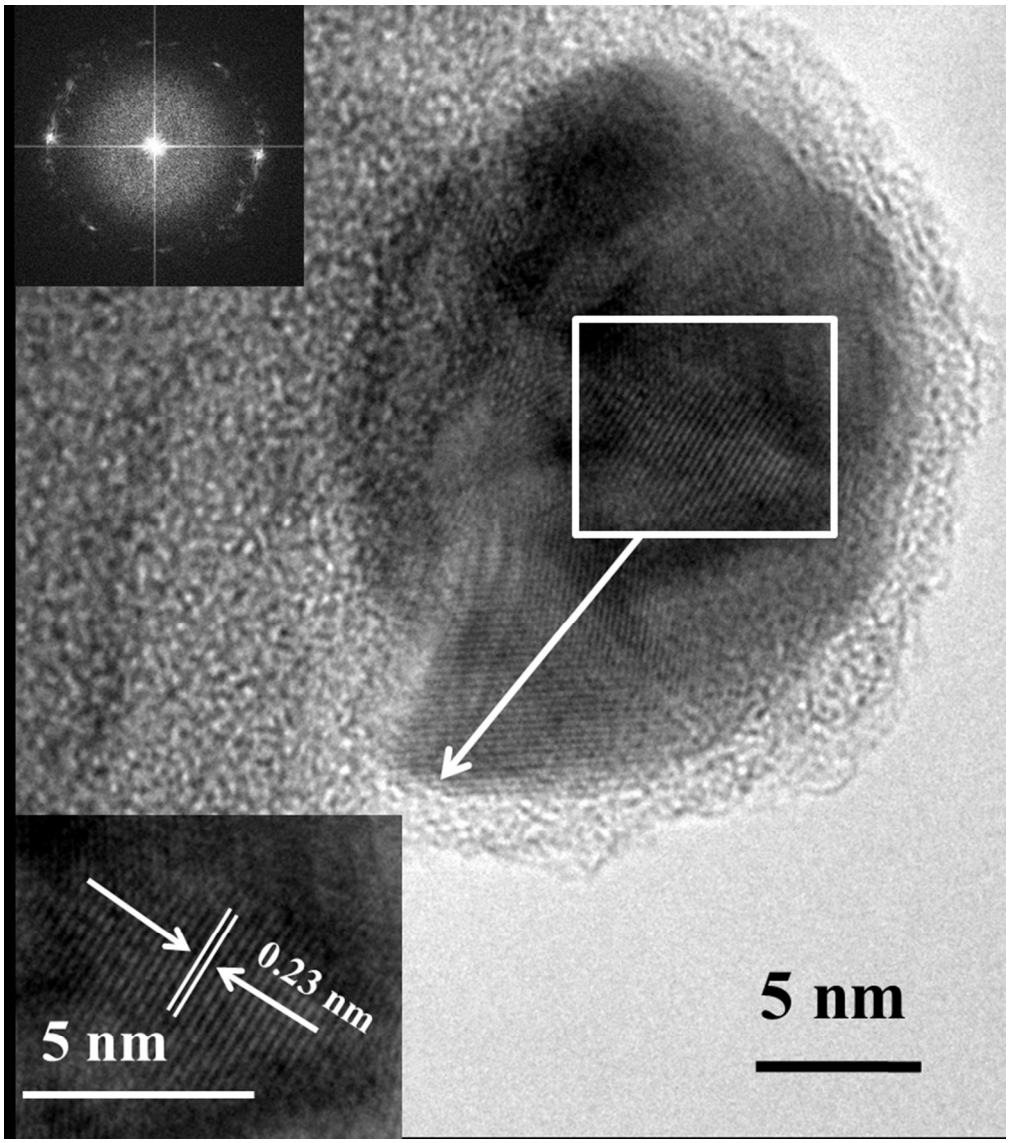

Fig. 2(c) TEM images of the products: Enlarged image of the Ag nanoparticle on the surface of carbon microspheres as indicated by square in (b) (Inset at the top left is electron diffraction pattern of corresponding Ag nanoparticle)
141x160mm (150 x 150 DPI)

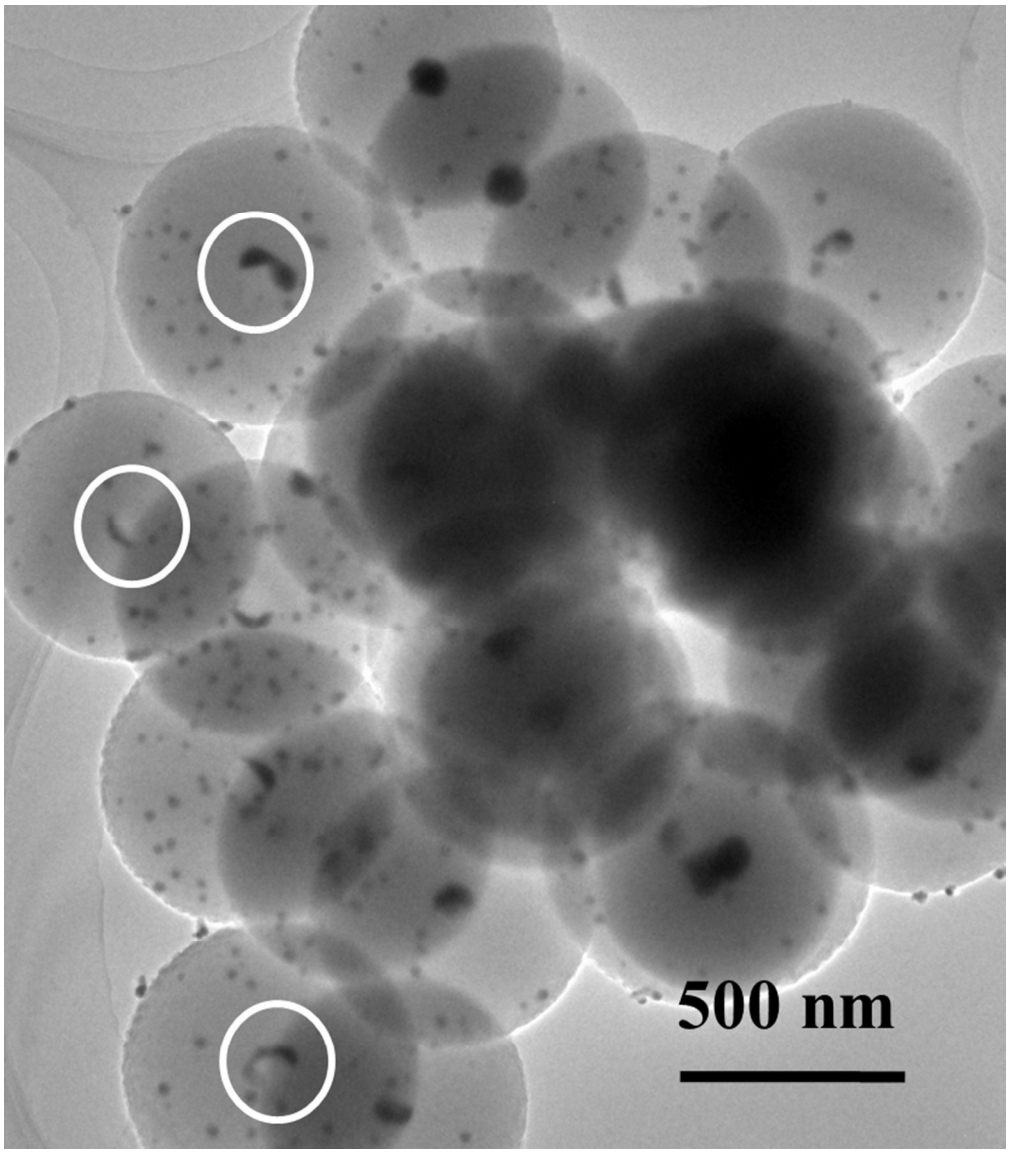

Fig. 2 (d) TEM images of the products:Carbon nanoparticles with hollow core or split Ag nanoparticle core as indicated by circle
140x160mm (150 x 150 DPI)

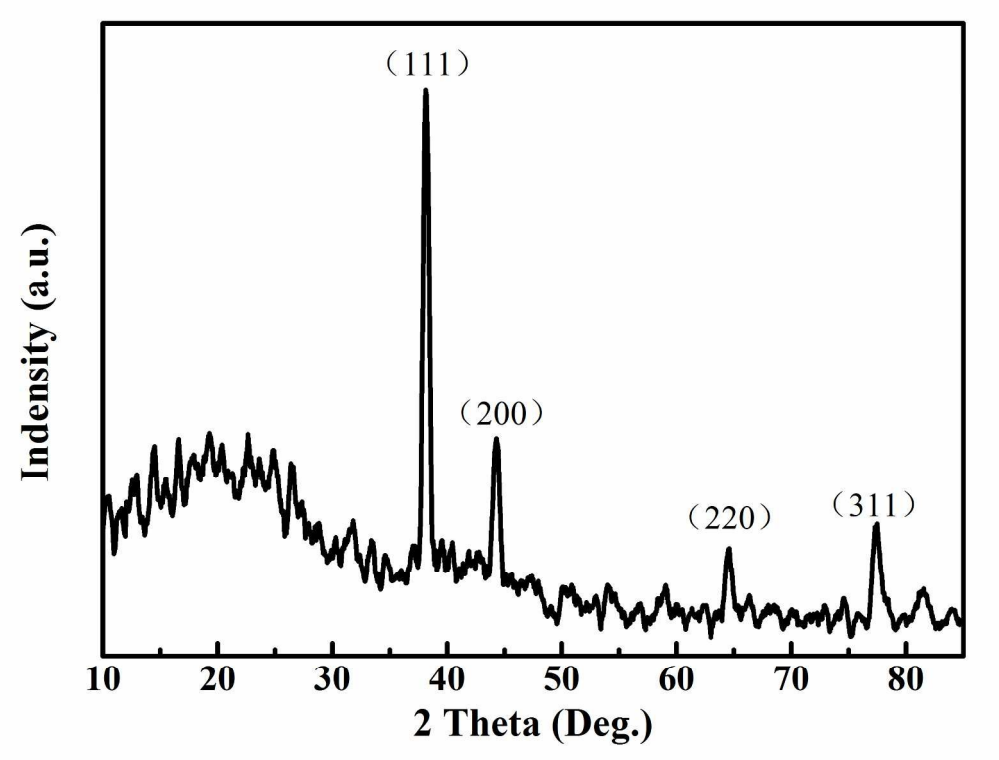

Fig. 3 XRD patterns of as-synthesized Ag-C-Ag NPs.
229x174mm (300 x 300 DPI)

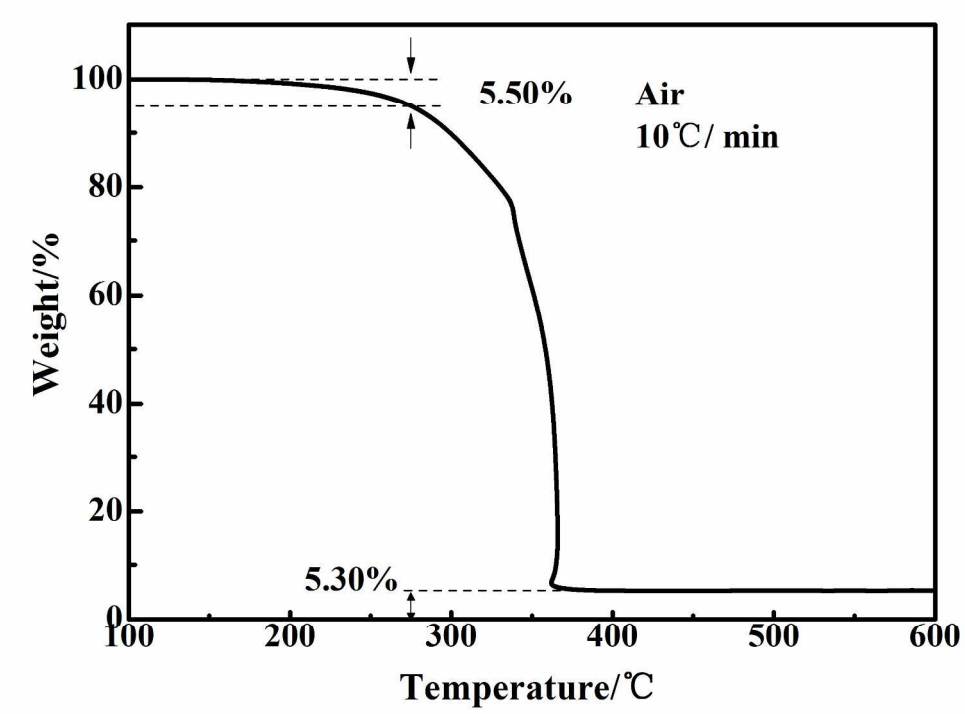

Fig. 4 TG curve of Ag-C-Ag NPs
243x178mm (300 x 300 DPI)

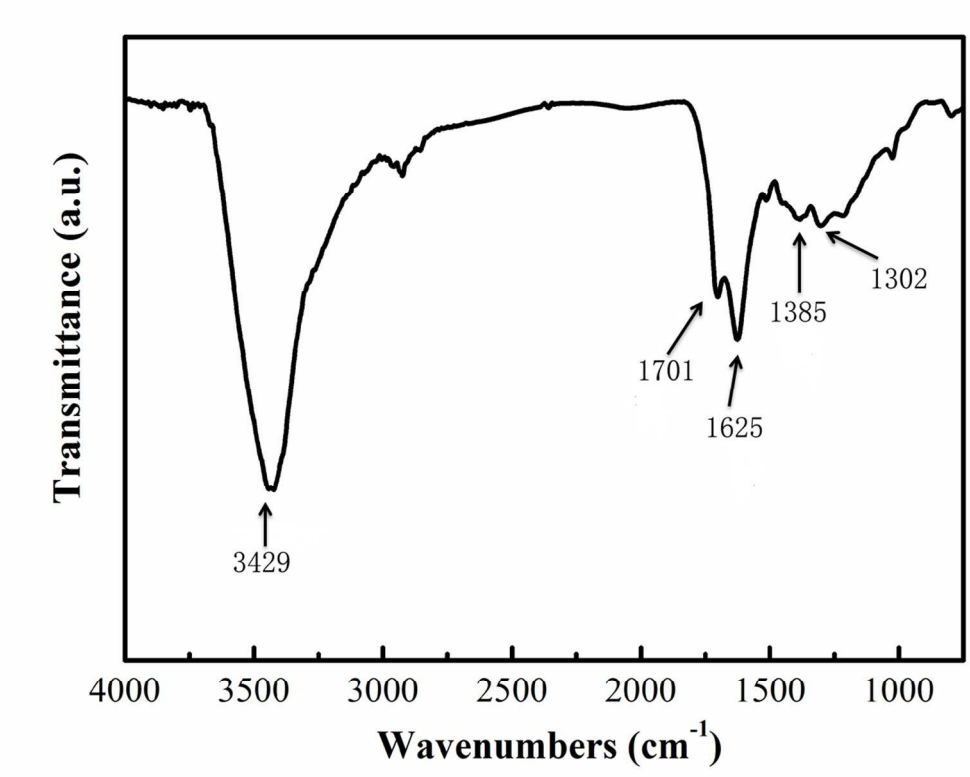

Fig. 5 FTIR spectra of Ag-C-Ag NPs
228x178mm (150 x 150 DPI)

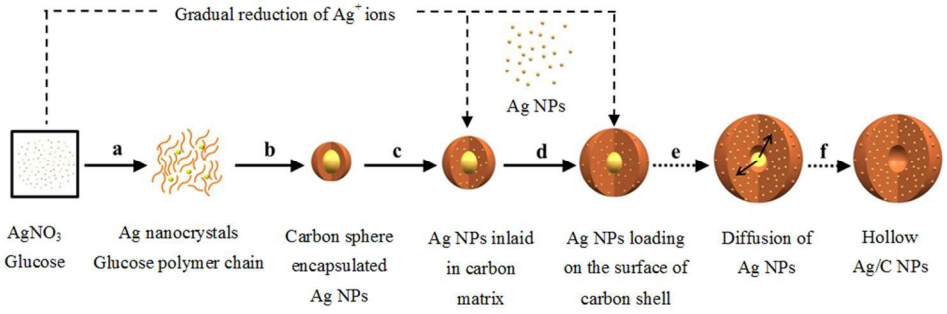

Fig. 6 The proposed growth mechanism of Ag-C-Ag NPs. (a) Reduction of Ag ions and polymerization of glucose; (b) Formation of Ag core and initiatory carbonization of glucose; (c) Ag nanoparticles were encapsulated in the carbon matrix during the further carbonization of glucose ; (d) Last reduced Ag nanoparticles were loaded on the surface; (e) Diffusion of Ag nanoparticle core; (f) Formation of hollow nanocomposites.
181x65mm (150 x 150 DPI)

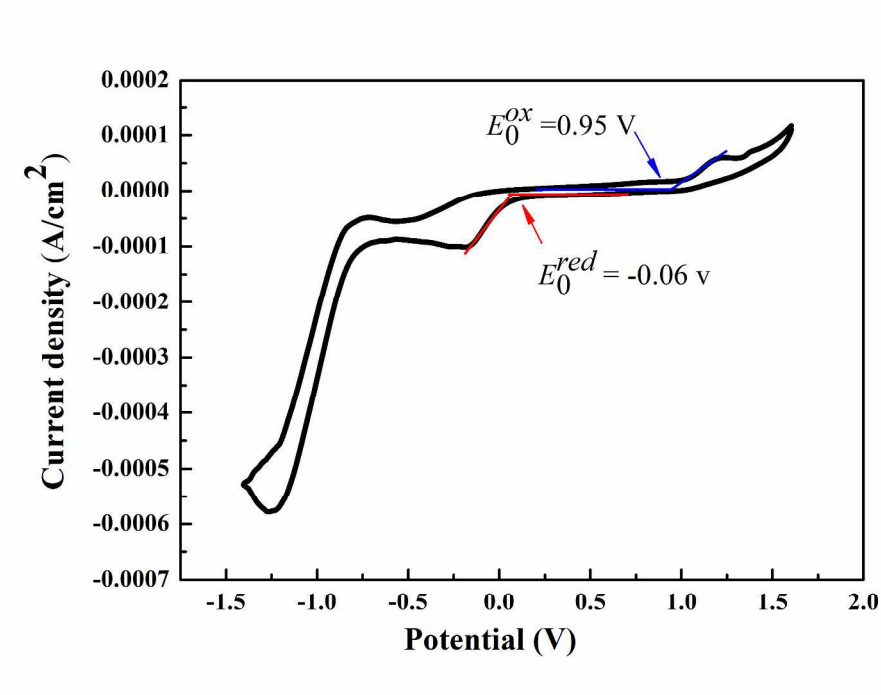

Fig. 7(a) CV curve of Ag@C NPs
286x199mm (300 x 300 DPI)

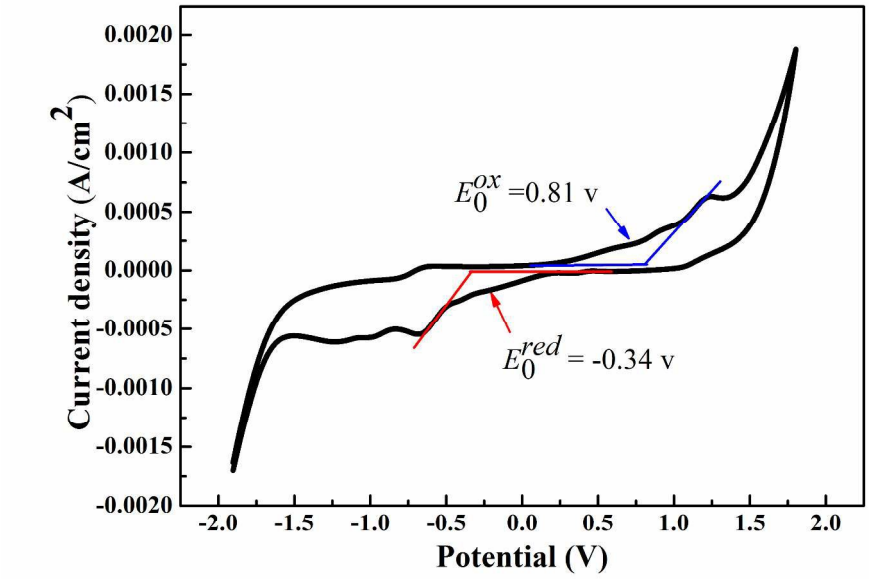

Fig. 7 (b) CV curve of Ag-C-Ag NPs,
286x199mm (300 x 300 DPI)

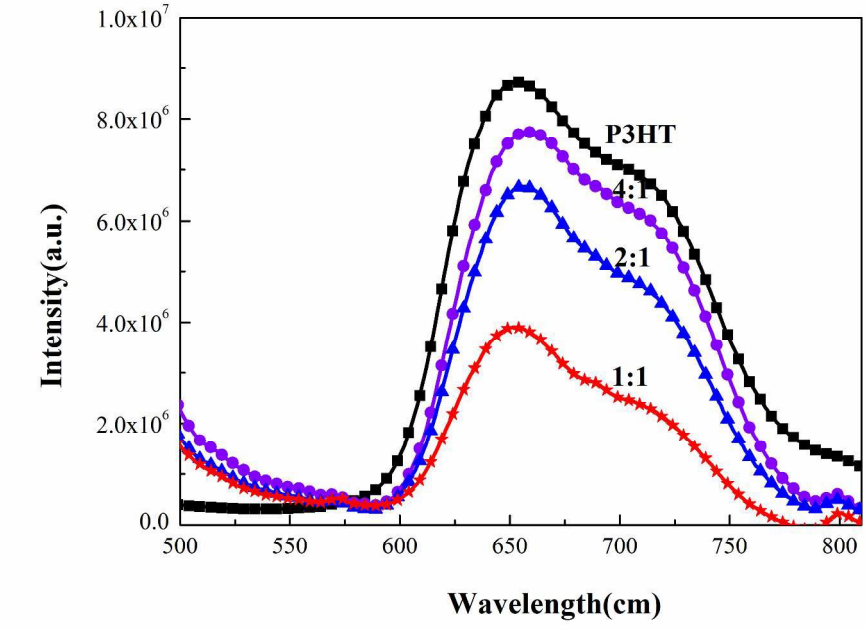

Fig. 8 The PL spectra of films with different P3HT:Ag-C-Ag ratio on glass substrates (Ex: 420 nm).
296x209mm (300 x 300 DPI)

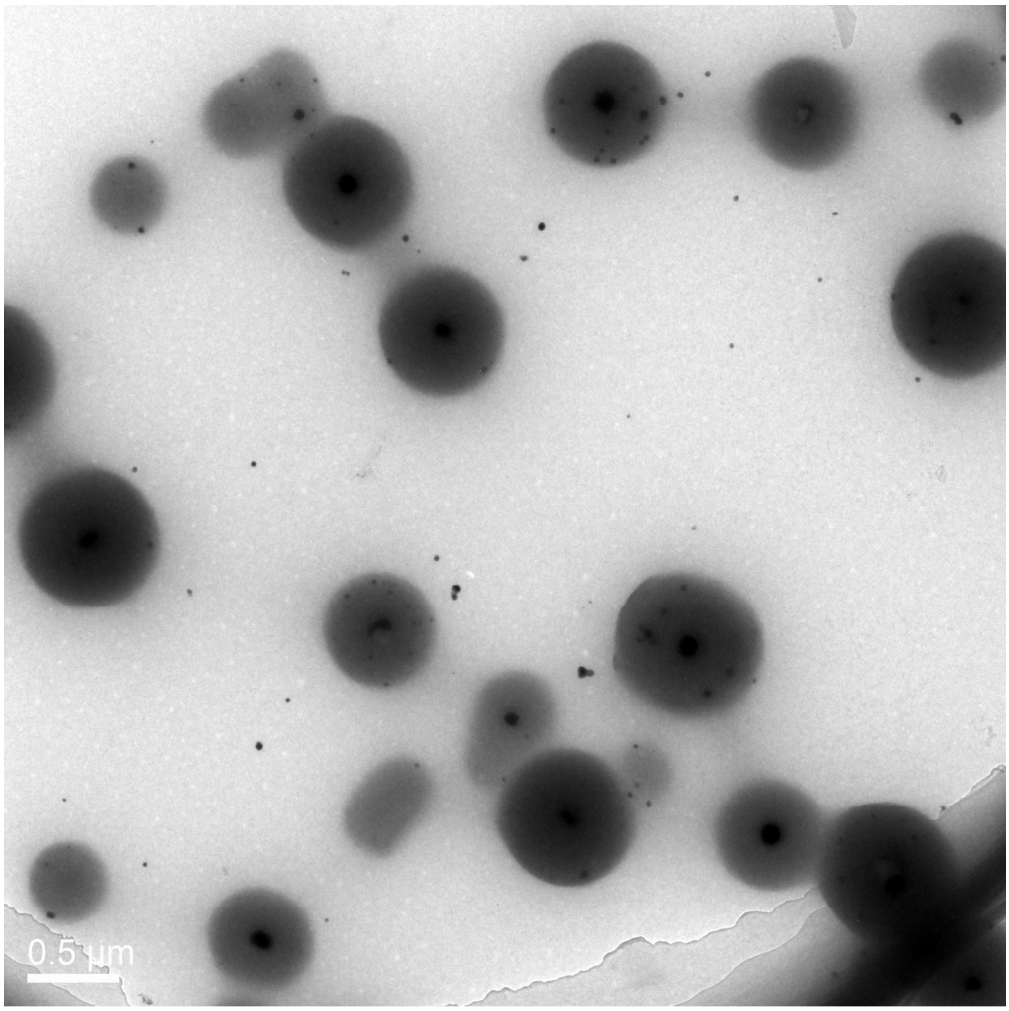

Fig. 9 TEM image of P3HT: Ag-C-Ag composite film (2:1, w:w).
722x722mm (72 x 72 DPI)

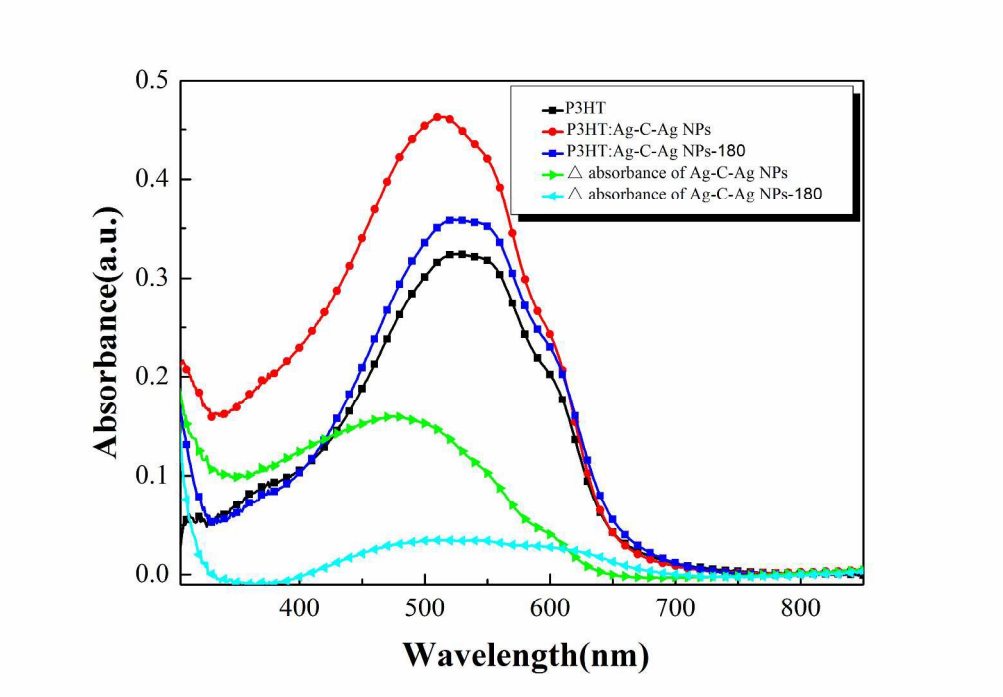

Fig. 10 The UV–Vis spectra of P3HT, P3HT:Ag-C-Ag NPs (2:1, w:w) and P3HT:Ag-C-Ag NPs-180 composite film (2:1, w:w).
287x201mm (300 x 300 DPI)

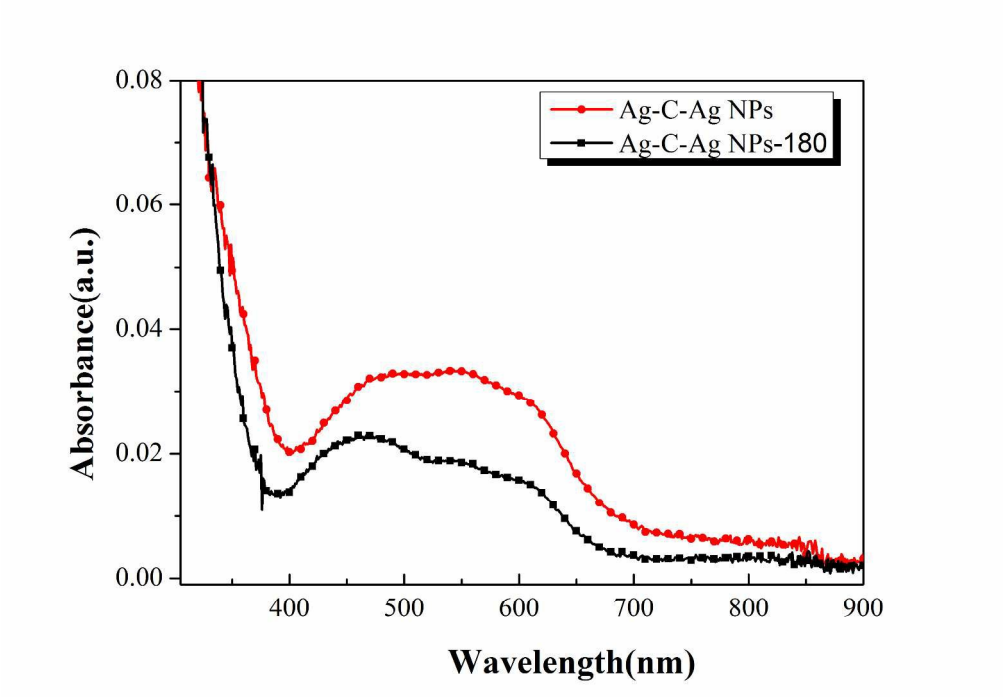

Fig. 11 The UV-Vis spectra of Ag-C-Ag NPs (5 mg/mL, 1000 rpm) and Ag-C-Ag NPs-180 (5 mg/mL, 1000 rpm).
287x201mm (300 x 300 DPI)